Pure appl. geophys. 163 (2006) 947–973
0033–4553/06/060947–27
DOI 10.1007/s00024-006-0061-y

Pure and Applied Geophysics

Quantifying Damage, Saturation and Anisotropy in Cracked Rocks by Inverting Elastic Wave Velocities

Alexandre Schubnel,[1] Philip M. Benson,[1,2] Ben D. Thompson,[1,3] Jim F. Hazzard,[1,4] and R. Paul Young[1]

Abstract—Crack damage results in a decrease of elastic wave velocities and in the development of anisotropy. Using non-interactive crack effective medium theory as a fundamental tool, we calculate dry and wet elastic properties of cracked rocks in terms of a crack density tensor, average crack aspect ratio and mean crack fabric orientation from the solid grains and fluid elastic properties. Using this same tool, we show that both the anisotropy and shear-wave splitting of elastic waves can be derived. Two simple crack distributions are considered for which the predicted anisotropy depends strongly on the saturation, reaching up to 60% in the dry case. Comparison with experimental data on two granites, a basalt and a marble, shows that the range of validity of the non-interactive effective medium theory model extends to a total crack density of approximately 0.5, considering symmetries up to orthorhombic. In the isotropic case, Kachanov's (1994) non-interactive effective medium model was used in order to invert elastic wave velocities and infer both crack density and aspect ratio evolutions. Inversions are stable and give coherent results in terms of crack density and aperture evolution. Crack density variations can be interpreted in terms of crack growth and/or changes of the crack surface contact areas as cracks are being closed or opened respectively. More importantly, the recovered evolution of aspect ratio shows an exponentially decreasing aspect ratio (and therefore aperture) with pressure, which has broader geophysical implications, in particular on fluid flow. The recovered evolution of aspect ratio is also consistent with current mechanical theories of crack closure. In the anisotropic cases—both transverse isotropic and orthorhombic symmetries were considered—anisotropy and saturation patterns were well reproduced by the modelling, and mean crack fabric orientations we recovered are consistent with *in situ* geophysical imaging.

Our results point out that: (1) It is possible to predict damage, anisotropy and saturation in terms of a crack density tensor and mean crack aspect ratio and orientation; (2) using well constrained wave velocity data, it is possible to extrapolate the contemporaneous evolution of crack density, anisotropy and saturation using wave velocity inversion as a tool; 3) using such an inversion tool opens the door in linking elastic properties, variations to permeability.

Key words: Elastic wave velocities, anisotropy, crack density, saturation, effective medium, attenuation, aspect ratio, Vp/Vs ratio, shear stress, effective pressure.

[1]Lassonde Institute, University of Toronto, 170 College Street, Toronto, ON M5S 3E3, Canada
[2]Mineral, Ice and Rock Physics Laboaratory, University College London, Gower Street, London, WC1E 6BT, UK
[3]Applied Seismology Laboratory, Department of Earth Sciences, Liverpool University, 4 Brownlow St., Liverpool, L69 3GP, UK
[4]Rocksciences Inc., 439 University Ave., Toronto, ON M5G 1Y8, Canada

1. Introduction

In upper-crustal conditions, fractures are ubiquitous (from major fault zones to continental shields) and present at all scales in rocks (from macroscopic fractures to microcracks). Despite the fact that these fractures generally represent only small amounts of porosity, they can exert considerable influence upon the rock physical properties (BRACE *et al.,* 1968) or even the fracture toughness (NASSERI *et al.,* this issue). In particular, the existence of embedded microcrack fabrics in rocks significantly influences the elastic properties (SIMMONS and BRACE, 1965; WALSH, 1965), contributes to the difference between static and dynamic elastic moduli (SIMMONS *et al.,* 1975; MAVKO and JIZBA, 1991) and aligned crack fabrics may produce elastic anisotropy (KERN, 1978; KERN *et al.,* 1997). When fluids are present, cracks also play a key role in making the rock permeable on a macroscopic scale. For such reasons, seismic data and velocity field analysis are used on a daily basis in the oil industry to quantify the oil content and the identify fluid properties, i.e., oil or gas. In seismotectonics, a key unanswered question is whether earthquakes and volcanic eruptions can be predicted by quantifying time dependent precursory damage accumulation using elastic wave velocity variations (CHUN *et al.,* 2004; VOLTI and CRAMPIN, 2003; GAO and CRAMPIN, 2004). Thus the understanding and quantification of elastic wave velocity variations is critical to extract information on the physical state of rocks from seismic and seismological data. This has major implications when considering the possible hydro-mechanical coupling taking place during the seismic cycle (MILLER, 2002), forecasting the life time of oil reservoirs, or the integrity of underground storage of hazardous wastes. In most cases, geophysicists have few means to retrieve information on the physical state of field rock masses, other than to invert elastic wave velocities into damage parameters.

For all those reasons, numerous models which predict properties of materials as a function of damage have been developed in the framework of Effective Medium Theories (EMT) in the last thirty years (ESHELBY, 1957; WALSH; 1965; O'CONNELL and BUDIANSKY, 1974, 1977; ANDERSON *et al.,* 1974; SOGA *et al.,* 1978; CHENG and TOKSÖZ, 1979; HUDSON, 1981, 1982, 1986; NISHIZAWA, 1982; KACHANOV, 1994; SAYERS and KACHANOV, 1991, 1995; LE RAVALEC and GUÉGUEN, 1996; SCHUBNEL and GUÉGUEN, 2003). Here, we report an approach based on KACHANOV's (1994) non-interactive EMT scheme which allows the straightforward inversion of elastic wave-velocity measurements made on several rock types in the laboratory into crack density, mean crack aspect ratio and mean crack fabric (or alignment). As the extensive laboratory input data compiled in this study were measured independently, our study provides an ideal opportunity to test the model applicability and investigate directly the elastic wave inversion results, in particular the evolution of crack density and mean crack aspect ratio with pressure and shear stress.

2. Effective Elastic Medium Containing Cracks

Statistically, the effective elastic properties of an initially isotropic medium depend on a few intrinsic parameters, including:

- the solid matrix elastic properties (Young's modulus E_o and Poisson ratio v_o).
- the fluid bulk modulus K_f and the level of fluid saturation.
- the crack density ρ defined as $\rho = \frac{1}{V}\sum^{N} c_i^3$ where c_i is the radius of the i-th crack, N being the total number of cracks embedded in the Representative Elementary Volume (REV) V.
- the crack geometry (in our case, we consider penny-shaped geometry (Figure 1a), their average aspect ratio $\zeta = \langle w/c \rangle$ and their spatial distributions.

The concept of crack density and mean aspect ratio is a statistical generalization of the concept of porosity for non-spherical inclusions since the crack porosity ϕ is defined as $\phi = \pi\rho\zeta$. In an isotropic matrix containing a uniform (isotropic) distribution of crack centers, the effective elastic modulus of a rock M^* is a linear function of the crack density that can be written in the form (first perturbation order):

$$\frac{M_o}{M^*} = 1 + h.\rho, \tag{1}$$

where M_o is the solid matrix elastic modulus and h is a positive scaling parameter that depends on the matrix and fluid properties, the geometry of the cracks and the interactions between them. Despite the facts that i) real fractures are not generally uniformly distributed spatially — a fractal-type description is often more realistic

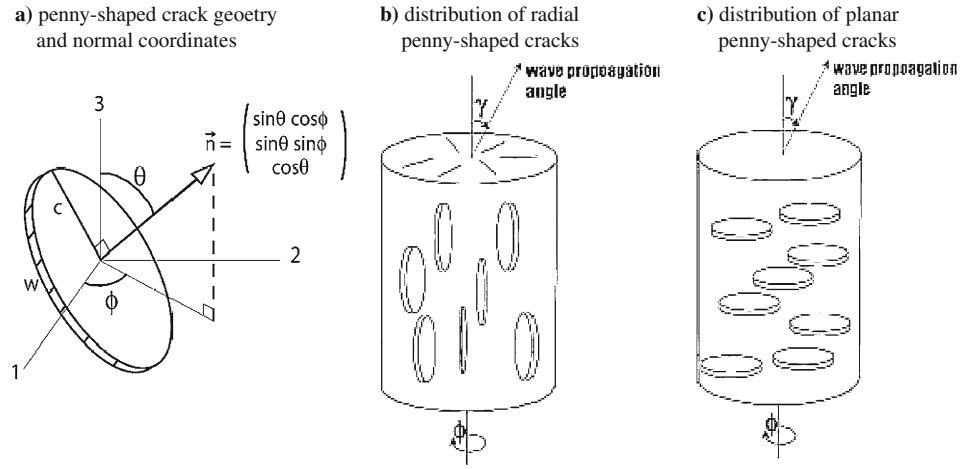

Figure 1 a)
Geometry, conventions and coordinates of a 3-D penny-shaped crack. The two crack distributions considered here: b) the case of radial penny-shaped cracks. c) the case of coplanar penny-shaped cracks.

(e.g., in some crystalline rocks, cracks can be very highly spatially concentrated, with intact rock between these zones), ii) real fractures have intersections and iii) real fractures also have shapes which are complex in detail, most EMT have been derived for non-intersecting cracks, uniform distributions of crack centers and simple crack geometries. Although those three important simplifications can be discussed from a theoretical point of view, considerable insight has been gained from them and the scalar h has been calculated by various authors for all kind of inclusion geometries (spherical, elliptical, penny-shaped discs, rectangular plates or linear cracks — see MAVKO *et al.,* 1998 for a good compilation) and fluid properties. These simplifications (non-intersecting 'penny-shaped' cracks and uniform distributions of crack centers) are used throughout this paper.

Recently, ORLOWSKY *et al.* (2003) and SAENGER *et al.* (2004) showed numerically that the best EMT scheme was the Differential Self-Consistent (DSC) theory (CLEARY *et al.,* 1980; BERRYMAN, 1992; LE RAVALEC and GUÉGUEN, 1996). However the accuracy of the DSC calculation has two main drawbacks: 1) it is limited to isotropic formulations and 2) the way the effective elastic moduli are calculated makes its use for elastic wave inversion complicated.

The most simple of all EMT is certainly the non-interactive theory because it neglects the problem of stress interactions between cracks and is therefore independent of crack centers distribution. It also allows easy computation of anisotropic fluid-filled crack distributions. Non-interactive EMT was shown to be valid when cracks are distributed randomly or when aligned (KACHANOV, 1994; SAYERS and KACHANOV, 1995; SCHUBNEL and GUÉGUEN, 2003) although ORLOWSKY *et al.* (2003) and SAENGER *et al.* (2004) have shown numerically that it would systematically overestimate the crack density. However, it has several advantages over other EMTs: i) it overcomes the divergence problems encountered in HUDSON's theory (HUDSON, 1981, 1982, 1986) or the non-physical drop of an elastic modulus to zero after a critical crack density encountered in the Self Consistent (SC) theory (O'CONNELL and BUDIANSKY, 1974, 1977, ANDERSON *et al.,* 1974; SOGA *et al.,* 1978); ii) any crack distribution can be computed easily, keeping in mind that results are best for aligned or randomly oriented cracks; iii) it depends both on the crack density and the mean crack aspect ratio; iv) and, most importantly, its easy formulation enables one to perform a direct inversion of elastic wave velocities into crack density and aspect ratio, as we will see in the next sections.

2.1 Non-interactive Formulation for Isotropically Distributed Cracks

When neglecting stress interactions between cracks, the effective elastic modulii of a cracked solid can be calculated exactly and rigorously in a unique manner that depends solely upon the crack orientations and distribution. Such a hypothesis is often wrongly confused with the low crack density approximation. Clearly, a low crack density means that cracks are (on average) distant from each other and the

non-interactive assumption is likely to be verified. At higher densities however, it is clear that cracks will interact with each other, both in terms of direct stress transfer and fluid flow between fractures (which will become more common with increasing crack densities). Nonetheless one should keep in mind (and this has been forgotten for example in both HUDSON's and the Self Consistent theory) that the stress field is is not only amplified at crack tips, but also shielded on the crack flanks. For such reasons, we can assume that stress interactions are partially compensating geometrically for certain distributions such as random (isotropic) or aligned crack distribution. KACHANOV (1994) showed numerically that the stress interactions in the case of intersecting cracks are small and that stress amplifications are shorter range than shielding. Finally and because of the non-intersecting assumption, EMTs are high-frequency (>KHz) theories for which squirt-flow mechanisms (MAVKO and JIZBA, 1975) can be neglected. It has been shown that, using all those assumptions, the non-interactive approximation gave reasonable and interpretable results at least up to crack densities of 0.5 (KACHANOV, 1994; SAYERS and KACHANOV, 1995; SCHUBNEL and GUÉGUEN, 2003; BENSON *et al.,* 2006).

In the non-interactive approximation, each crack is considered to be isolated and the elastic perturbation ΔS_{ijkl} compliance due to cracks is simply the sum of each crack contribution. Since the average bulk elastic strain is the sum of the matrix elastic strain and the superposition of elastic strain of each individual crack, effective elastic modulii can simply be calculated using the elastic potential f (KACHANOV, 1994; SAYERS and KACHANOV, 1995). In the isotropic case, KACHANOV (1994) showed that the effective Young E^* and shear modulii μ^* of a rock could be written[1] as:

$$\frac{E_o}{E^*} = 1 + \left(1 + \frac{3}{5}\left[\left(1 - \frac{v_o}{2}\right)\left(\frac{\delta}{1+\delta} - 1\right)\right]\right)h\rho \tag{2}$$

and:

$$\frac{\mu_o}{\mu^*} = 1 + \left(1 + \frac{2}{5}\left[\left(1 - \frac{v_o}{2}\right)\left(\frac{\delta}{1+\delta} - 1\right)\right]\right)\frac{h\rho}{(1+v_o)}, \tag{3}$$

where h is a geometrical factor linked to the penny-shaped geometry (see Appendix I) and given by,

$$h = \frac{16(1 - v_o^2)}{9(1 - v_o/2)}. \tag{4}$$

δ is a non-dimensional number which characterizes the coupling between the stress and the fluid pressure, and is equal to:

[1] Note that equation (3) has been corrected from KACHANOV's (1994) original manuscript by FORTIN (2005) and BENSON *et al.* (2006).

$$\delta = (1 - v_o/2)\frac{E_0\zeta}{K_f}h. \tag{5}$$

δ compares the fluid bulk modulus K_f to the crack bulk modulus $\{(1 - v_o/2)E_o\zeta h\}$ assuming that all change in the crack volume is due to aperture variations (see Appendix I). As a lower bound, i.e., for an incompressible fluid such as water, and using $E_0 \sim 5.10^{10}$, $\delta \to 0$ and is negligible if ζ is small ($<10^{-3}$). As an upper bound, i.e., for a compressible fluid such as dry air, δ considerably exceeds 1 and $\delta/1 + \delta \to 0$.

Figures 2a and 2b present the normalized P- and S- wave velocity isocontours respectively as a function of both crack density and the aspect ratio. The velocities were calculated from equations (2)–(3) using solid matrix and fluid elastic parameters typical of an undamaged water saturated granite and equal to: $E_o = 85$ GPa, $v_o = 0.25$ and $K_f = 2$ GPa. Velocities were normalized to the crack-free velocities (i.e., $\rho = 0$) to remove bulk density effects. On Figure 2a, the *P*-wave velocity is shown to decrease with crack density. However, at a given crack density, *P*-wave velocity remains more or less constant with aspect ratio. On the contrary, whilst *S*-wave velocity also decreases with crack density on Figure 2b, they are very sensitive to the crack mean aspect ratio. Figure 2c shows that the evolution of the Vp/Vs ratio is a function of both crack density and aspect ratio when cracks are saturated with fluid. This way, KACHANOV's (1994) non-interactive model permits the quantification of both the crack density ρ and the aspect ratio ζ, through the saturation coefficient δ (equation 5). As a direct consequence, one can expect to be able to extract from Vp and Vs measurements in saturated rocks containing cracks, not only the crack density, but also the aspect ratio.

2.2 Non-interactive Formulation: General Case

In the most general case, when fractures seem to be aligned in one or several directions and wavelengths are considerably larger than the fracture spacing, it is convenient to formulate the equivalent anisotropic medium problem in terms of compliances (KACHANOV, 1994; SAYERS and KACHANOV, 1995; SCHOENBERG and SAYERS, 1995). For an isotropic matrix containing penny-shaped cracks, the additional elastic compliance ΔS_{ijkl} due to those can be expressed as (SAYERS and KACHANOV, 1995):

$$\Delta S_{ijkl} = \frac{1}{4hE_o}(\delta_{ik}\alpha_{jl} + \delta_{il}\alpha_{jk} + \delta_{jk}\alpha_{il} + \delta_{jl}\alpha_{ik}) + \beta_{ijkl} \tag{6}$$

where α_{ij} is the crack density tensor:

$$\alpha_{ij} = \rho.\langle n_i n_j \rangle \tag{7}$$

and β_{ijkl} the saturation tensor:

$$\beta_{ijkl} = \rho.\left[\left(1 - \frac{v_0}{2}\right)\frac{\delta}{1+\delta} - 1\right]\langle n_i n_j n_k n_l \rangle. \tag{8}$$

δ_{ij} is the Kronecker symbol and we recall that the scalar (or total) crack density is equal to $\rho = \mathrm{tr}(\alpha) = Nc^3/V$. In the case of an orthorhombic crack distribution, the crack density tensor is diagonal, and it follows from equations (6)–(8) that the nine independent effective elastic compliances can be expressed:

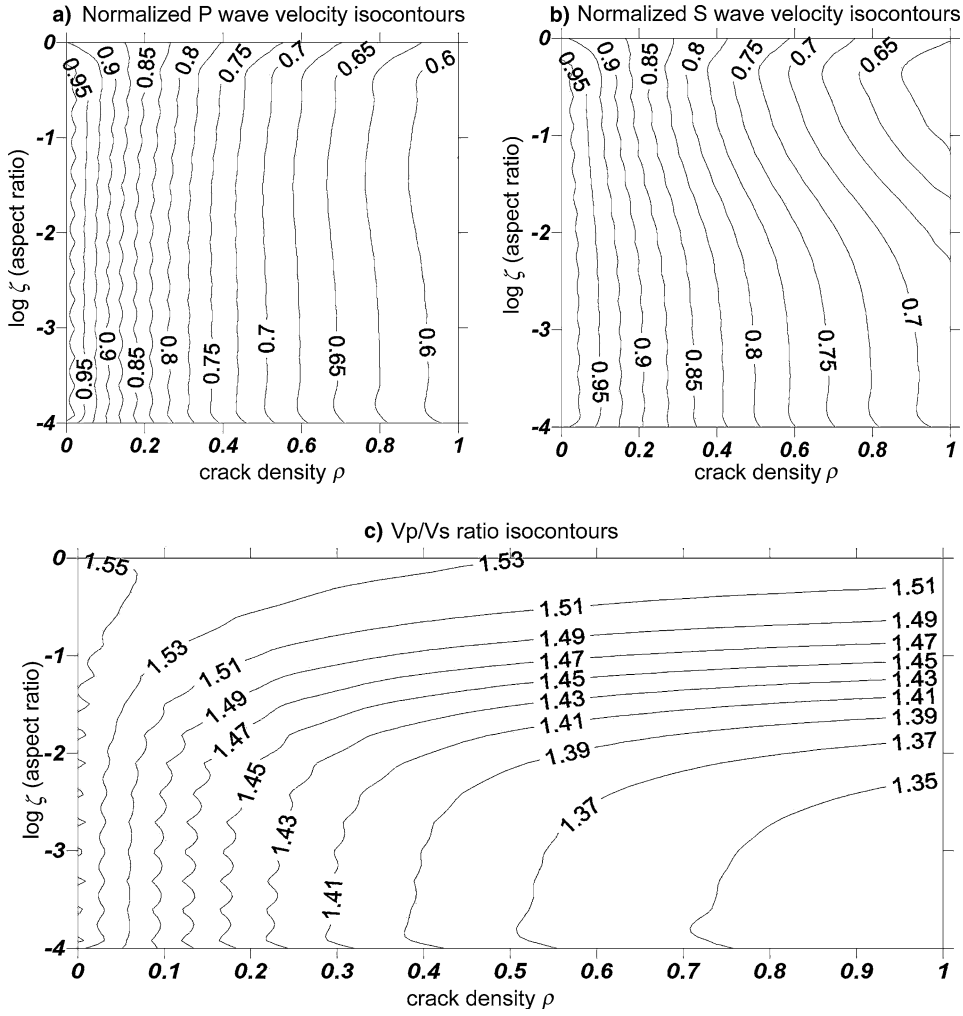

Figure 2

Isotropic case: Elastic wave velocities calculated from equations (2)–(3) using solid matrix and fluid elastic parameters typical of a water saturated granite and equal to: $E_o = 85$ GPa, $v_o = 0.25$ and $K_f = 2$ GPa. a) and b) normalized *P*- and *S*-wave velocity isocontours as a function of crack density and aspect ratio. Velocities were normalized to the crack free velocities (i.e., $\rho = 0$) to remove bulk density effects. c) evolution of the Vp/Vs ratio as a function of both crack density and aspect ratio.

$$S_{ijkl} = \begin{cases} = S^o_{ijkl} + \frac{\rho}{E_o h}\left(\langle n_i^2\rangle + \left[(1-\frac{v_0}{2})\frac{\delta}{1+\delta} - 1)\right]\langle n_i^4\rangle\right) if\ \{i=j=k=l\} \\ = S^o_{ijkl} + \frac{\rho}{E_o h}\left(\frac{\langle n_i^2\rangle + \langle n_j^2\rangle}{4} + \left[(1-\frac{v_0}{2})\frac{\delta}{1+\delta} - 1)\right]\langle n_i^2 n_j^2\rangle\right) if\ \{i=k \quad \text{and} \quad j=l\} \\ = S^o_{ijkl} + \frac{\rho}{E_o h}\left[(1-\frac{v_0}{2})\frac{\delta}{1+\delta} - 1)\right]\langle n_i^2 n_k^2\rangle \text{ if } \{i=j \quad \text{and} \quad k=l\} \end{cases} \quad (9)$$

Recalling the relationship between dependent elastic compliances, the formulation for transverse isotropy can also be obtained from equation (9). Assuming now a continuous distribution function of crack orientations, the average i-th component of the crack fabric can be defined as follows:

$$\langle n_i\rangle = \frac{1}{2\pi}\int_0^{2\pi} d\phi \int_0^{\pi/2} \psi(\theta,\phi) n_i \sin\theta d\theta \ , \quad (10)$$

$\psi(\theta,\phi)$ being the orientation distribution function (cf. fig. 1a). The tensors $\langle n_i n_j\rangle$ and $\langle n_i n_j n_k n_l\rangle$, which represent respectively the second-order and the fourth-order moments of the crack orientation distribution function respectively, can be calculated easily in the same way.

2.3 Wet and Dry Elastic Waves Anisotropy: Numerical Results

For the sake of simplicity, we will consider Dirac distributions, so that $\langle n_i\rangle = n_i$ and subsequently, in such a way that the average crack fabric orientation is described as on Figure 1a for a single crack. In this section, we consider two different types of crack distributions: i) radial cracks ($n_3 = 0, n_1 = n_2 = 1/\sqrt{2}$) and ii) planar cracks ($n_3 = 1, n_1 = n_2 = 0$). The first case corresponds to a distribution of symmetrically distributed radial cracks (symmetry along the vertical axis, cracks normal in the horizontal axis) and is representative of the TI symmetry (Fig. 1b). The second case corresponds to horizontally aligned coplanar penny-shaped cracks and is representative of both TI and orthorhombic symmetry (Fig. 1c). Furthermore, only the lower and upper bound of saturation, i.e., for an incompressible fluid such as water $\delta \to 0$ and for a compressible fluid such as dry air, $\delta/1+\delta \to 0$, were investigated. In all that follows, the solid matrix Young's modulus and Poisson ratio were taken as equal to the ones of an isotropic and crack-free granite material, i.e., $E_o = 85$ GPa and $v_o = 0.25$, respectively.

2.3.1 Radial cracks

The case of radial cracks is illustrated on Figure 3. Figures 3a and 3b show the normalized P velocities versus the angle of propagation γ of the elastic wave, in wet and dry conditions respectively, and for crack densities equal to 0.1, 0.25, 0.5 and 1. The angle γ is defined as that between the vertical axis Ox_3 and the wave vector. For example, elastic waves propagating at 0 and 90 degrees correspond to propagation along the vertical and horizontal axes, respectively. The normalized wave velocity is

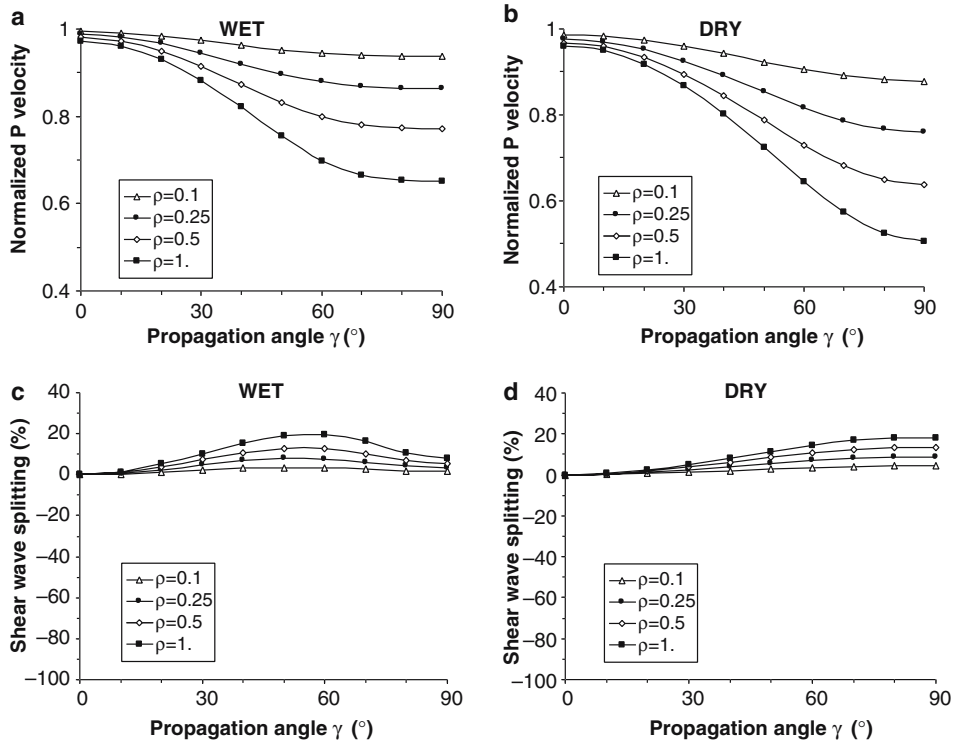

Figure 3

Case of radial cracks (Fig. 1b). Only the lower ($\delta \to 0$) and upper ($\delta/1+\delta \to 0$) bound of saturation were investigated using equation (9). The solid matrix Young's modulus and Poisson ratio were taken as equal to $E_o = 85$ GPa and $v_o = 0.25$, respectively. Velocities were normalized to the crack-free velocities (i.e., $\rho = 0$) to remove bulk density effects. Results are displayed for crack densities equal to 0.1 (open triangles), 0.25 (plain circles), 0.5 (open diamonds) and 1 (plain squares). a) and b) show the normalized *P*-wave velocity as a function of the direction of propagation γ in the wet and dry cases respectively. c) and d) show the shear-wave splitting ($\frac{SV(\gamma)-SH(\gamma)}{SV(\gamma)} * 100$ or birefringence) as a function of the direction of propagation γ in the wet and dry cases, respectively.

the ratio of V_γ to the solid grain velocity. In the case of radial cracks, *P* waves propagating vertically are unaffected and do not "see" the cracks. Anisotropy is larger in the dry case (up to 50% in the dry case, up to $\sim$ 40% in the wet case) but the pattern is very comparable in both cases. Figures 3c and 3d show the results obtained in terms of the shear-wave splitting $\left(\frac{SV(\gamma)-SH(\gamma)}{SV(\gamma)} * 100 \text{ or birefringence}\right)$ between vertically (SV) and horizontally (SH) polarized *S* waves in the wet and dry cases, respectively. In the dry case, SV waves always travel faster than SH. In the wet case, maximum splitting is observed at a γ angle of 60 degrees, whereas maximum dry splitting is obtained for horizontally propagating *S* waves. However, and as one could expect for a set of radial cracks, the effect of fluid is rather small.

2.3.2 Planar cracks

Figure 4 shows numerical results obtained in the case of planar cracks. Figures 4a and 4b present the normalized P velocities as a function of propagation angle γ and crack density in the wet and the dry cases, respectively. As noted earlier, the effect of cracks is considerably stronger in the dry case than in the wet case. This time, cracks are "invisible" to waves propagating in the horizontal direction ($\gamma = 90^o$); and in the dry case (Fig. 4b), the P-wave velocity decrease is very large (up to 60%) for waves propagating vertically, which is expected from geometrical considerations. However, and because the fluid is assumed to be fully incompressible, cracks are also "invisible" in the direction $\gamma = 0^o$ in the wet case (Fig. 4a). This can be explained theoretically as in KACHANOV's model, the normal crack compliance is assumed to be equal to zero

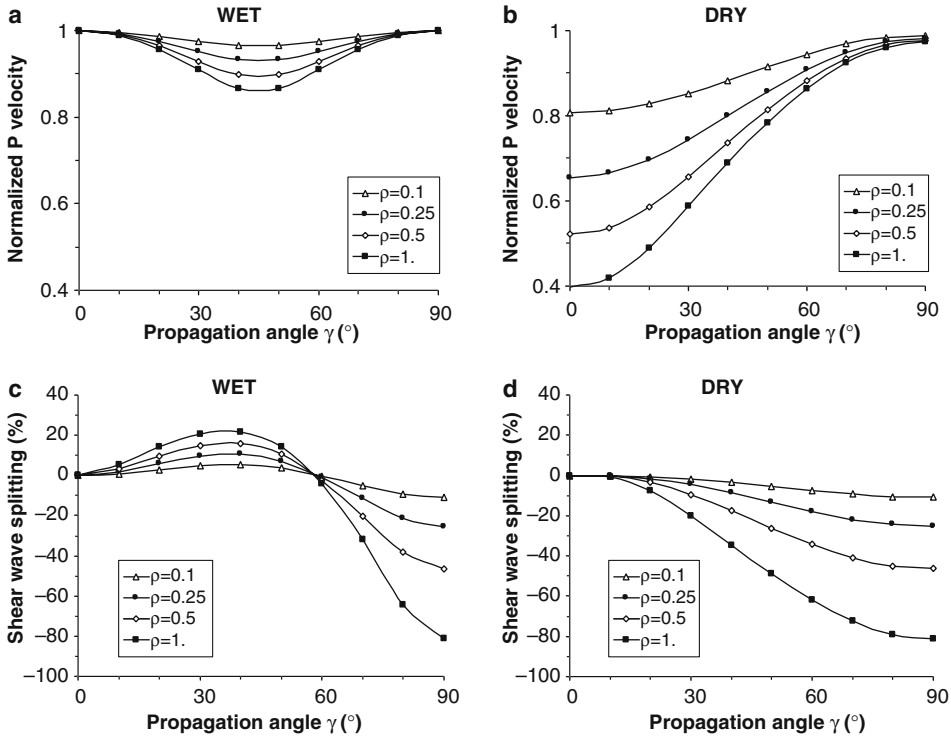

Figure 4

Case of coplanar cracks (Fig. 1c). Only the lower ($\delta \to 0$) and upper ($\delta/1 + \delta \to 0$) bound of saturation were investigated using equation (9). The solid matrix Young's modulus and Poisson ratio were taken as equal to $E_o = 85$ GPa and $v_o = 0.25$, respectively. Velocities were normalized to the crack free velocities (i.e., $\rho = 0$) to remove bulk density effects. Results are displayed for crack densities equal to 0.1 (open triangles), 0.25 (plain circles), 0.5 (open diamonds) and 1 (plain squares). a) and b) show the normalized P-wave velocity as a function of the direction of propagation γ in the wet and dry cases, respectively. c) and d) show the shear-wave splitting ($SV(\gamma) - SH(\gamma)/SV(\gamma) * 100$ or birefringence) as a function of the direction of propagation γ in the wet and dry cases, respectively.

(see Appendix I) when the fluid is fully incompressible (or when the crack is fully constrained). Therefore, in the wet case, the maximum anisotropy (up to 20% for $\rho = 1$) is seen for waves propagating at 45 degrees from the vertical, for which the associated shear strain is maximum. Figures 4c and 4d show the predicted results for shear-wave splitting ($SV(\gamma) - SH(\gamma)/SV(\gamma) * 100$). Again, the pattern is very different in the wet and the dry cases. As expected, in the dry case SH waves always propagate faster than SV waves. In the wet case however, and for propagation angles between 0 and 60 degrees, SV waves are faster than SH waves. Conversely, SH-wave velocity is higher than SV-wave velocity for angles larger than 60 degrees. The shear-wave splitting maximum observed is thus an effect of fluid incompressibility.

In each of the two distributions discussed above, the non-interactive model manifests a clear difference between dry and fully saturated cracks, both for *P* waves and *S* waves. Intermediate results for partial saturation could be obtained considering the δ parameter and average crack aspect ratio. It demonstrates that, to a certain extent, the *P*-wave anisotropy and *S*-wave birefringence patterns can correspond to a genuine crack distribution and saturation state. Therefore, combining velocity data on *P*-wave anisotropy and *S*-wave birefringence should allow one to investigate the "average" crack distribution in a rock, as well as the saturation state. Unfortunately, such extensive wave-velocity data is very rare in the literature. It exists at the field scale, however one would need to take into account the dispersion effects due to frequency and "squirt flow" mechanisms (MAVKO and NUR, 1975). This may be done using BIOT-GASSMANN or BROWN and KORRINGA's equations (1975), as shown by SCHUBNEL and GUÉGUEN (2003).

3. Inversion of Experimental Data

In the laboratory, experimental studies measuring the evolution of dynamic elastic properties under conditions simulating upper crust burial depths can be performed thanks to the use of piezoelectrics transducers (PZT), for which eigen-frequencies are generally well into the dynamic range (>100 KHz). Despite the experimental difficulties, such studies have been undertaken and can provide 'well-constrained' experimental datasets which are perfectly suited to attempt predicting the evolution of rock fabric parameters such as crack density, aspect ratio and alignment.

When modelling the evolution of elastic velocities, we restricted ourselves to the case of an initially isotropic solid rock matrix. The crack distribution function obeyed either an isotropic, transverse isotropic or orthorhombic symmetry. In such conditions, the effective elastic properties predicted by equations (2), (3) and (9) are dependent only upon the matrix Young's modulus E_o and Poisson ratio v_o, and more importantly, the scalar crack density ρ. Additionally, when cracks are non-randomly oriented, elastic wave velocities also depend on the mean orientation (θ, ϕ — Fig. 1a)

of the crack fabric with respect to the axis of symmetry. Finally, when saturated, elastic properties also depend on the saturation coefficient δ and therefore the average crack aspect ratio ζ and fluid bulk modulus K_f. In the following, we simply performed least-square inversions of laboratory datasets:

$$\mathrm{RMS}_i = \frac{1}{N_i}\sum_{N_i}(V_\gamma^{\mathrm{data}} - V_\gamma^{\mathrm{model}}(\rho,\zeta,\theta,\phi))^2 \tag{11}$$

in order to recover the crack density, average crack aspect ratio and orientation. Inversions were performed using initial *P*- and *S*- wave velocities of the "uncracked" material as calculated from experimental and/or petrological considerations, thus reflecting the average bulk solid matrix elastic properties. Model elastic wave-velocity field was calculated from equations (2), (3) and (9) as a function of ρ, ζ when the rock was saturated with water together with θ and ϕ when the rock was anisotropic. Each modelled velocity field was then compared using a simple RMS technique (equation 11) with experimental measurements. In equation (11), N_i represents the number of *P*- and *S*- velocity measurements along several γ directions at each step i of a given experiment. The lowest RMS error between modelled and data velocities was taken as being the best inversion result, which output the quadruplet (ρ,ζ,θ,ϕ). The agreement between data and best fit velocities is, in general, very good with the average error between model and data points lower than 0.05 km/sec. This is a direct consequence of the well constrained laboratory data itself.

3.1 Isotropic Inversions

Elastic wave velocities have been widely shown to increase with increasing hydrostatic pressure, because of crack closure. Conversely and in the presence of shear stress, elastic wave velocities can decrease due to nucleation and propagation of new microcracks. In the following, we compile experimental results obtained on two different rock types, representative of contrasting isotropic microcrack fabric, a porphyritic alkali basalt from Mount Etna and Carrara marble.

3.1.1 Crack density and aspect ratio evolution as a function of hydrostatic pressure

In the case of the Etnean basalt, the simultaneous evolutions of *P*- and *S*- wave elastic wave velocities were measured during hydrostatic compression of three different rock samples (38.1 mm diameter by 40 mm length) cored in three orthogonal directions (Fig. 5a). The measurements, performed in a high pressure confining cell installed at University College London (BENSON, 2004; BENSON *et al.*, 2005), evidenced no marked elastic anisotropy in the rock. The experimental *P*-wave velocities ranged from 5.35 ± 0.13 km/s at 5 MPa to 5.88 ± 0.12 km/s at 80 MPa; while *S*-wave velocities ranged from 3.30 ± 0.04 km/s to 3.60 ± 0.04 km/s. *P* and *S* elastic wavespeeds were inverted using equations (2) and (3). Crack-free elastic wave

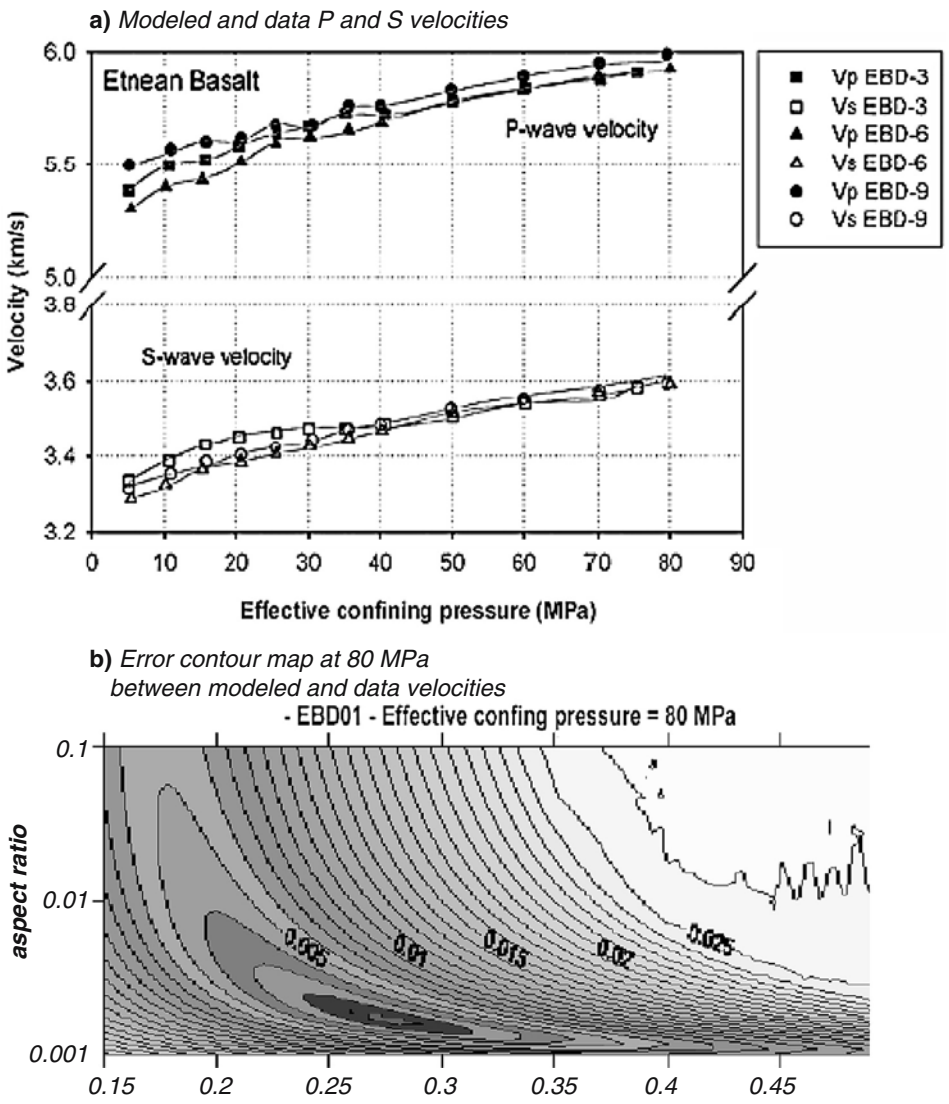

Figure 5

a) Modelled (solid lines) P and S velocities in Etna basalt compared to the laboratory measurements (dots - Benson *et al.*, 2005). The effective confining pressure was calculated as $P_c - P_p$ where P_c is the confining pressure and P_p the pore pressure. b) Error contour map between modelled and data (P and S) velocities in the case of sample EBD01 at 80 MPa confining pressure. Error contours are displayed as a function of crack density and aspect ratio, respectively. Darker areas represent lower errors.

velocities were taken as equal to $V_p = 6400\,\mathrm{m/s}$ and $V_s = 3750\,\mathrm{m/s}$ (i.e., solid matrix elastic parameter equal to $E = 100$ GPa and $v = 0.22$). The fluid bulk modulus was taken as $K_f = 2$ GPa.

Figure 5a compares the model *P* and *S* elastic velocities (solid and dashed line) to the experimental results (symbols). Because the degree of freedom of the inversion is zero (i.e., *P*- and *S*-wave velocities were modelled using only two distinct parameters: crack density and aspect ratio), the fit appears perfect, well below the experimental error bar. Figure 5b presents the error contour maps between modelled and data velocities as a function of crack density and aspect ratio for sample EBD01 at 80 MPa, respectively. As illustrated, the inversion is stable as only one minima can be distinguished and for a wave-velocity doublet (*P*,*S*) corresponds a unique solution for the crack density and aspect ratio doublet (ρ, ζ). As an output, the model gives back the evolution of parameters (ρ, ζ) with confining pressure which are displayed on Figures 6a and 6b. Results from the inversion reveal a decrease in crack density from ~ 0.5 to ~ 0.35 during pressurization, while the average crack aspect ratio decreases by one order of magnitude approximately. The decrease in crack density illustrates a decrease in the cracks apparent radii *c* as crack density evolves with $\sim c^3$. This is generally attributed to an increase of the crack surfaces contact areas as cracks are being closed. More importantly, the recovered evolution of aspect ratio shows an exponentially decreasing aspect ratio with confining pressure (and thus aperture evolution as the radius is not expected to vary much). The drop of one order of magnitude within the first MPa's is consistent with that expected intuitively, i.e., fast elastic crack closure at low pressures. This is also consistent with current theories on crack closure (KASELOW and SHAPIRO, 2004) where crack closure is generally modelled using an exponentially decreasing law with pressure with varying power exponents. One should note that the elastic wave inversion not only interprets the increase in both *P* and *S* velocities in terms of crack density consistently, but also the fact that the ratio *P*/*S* is changing in terms of aspect ratio reduction. This is probably one of the key advantages in using KACHANOV's (1994) scheme when modelling elastic properties in isotropy.

3.1.2 Crack density and aspect ratio evolution as a function of shear stress

Carrara marble is a well investigated marble, with coarse grainsize (150 μm) and a very low initial anisotropy (<1%). SCHUBNEL *et al.* (2005) measured both *P*- and *S*- wave velocities during a full tri-axial cycle in wet conditions ($Pc = 260$ MPa and $Pp = 10$ MPa). In this case, the non-interactive scheme becomes particularly relevant as calcite behaves plastically and intragranular plasticity inhibits long-range stress interactions between cracks. Initial *P*- wave velocity was equal to 5.9 km.s^{-1} $\pm$ 1% while final *P*-wave velocity was lower than 3 km.s^{-1} $\pm$ 1%. Figure 7a presents the evolution of both *P*- and *S*-wave velocities as a function of effective mean stress $\mathbf{P} = [(\sigma_1 + 2\sigma_3)/3 - P_p]$. In the first phase both velocities increased. When the onset of crack propagation was reached, *P*- and *S*-wave velocities began to decrease rapidly due to damage accumulation. During the subsequent relaxation period, wave velocities increased again, before decreasing drastically due to stress relief microcracking as hydrostatic stress was removed. On the figure, the fit between

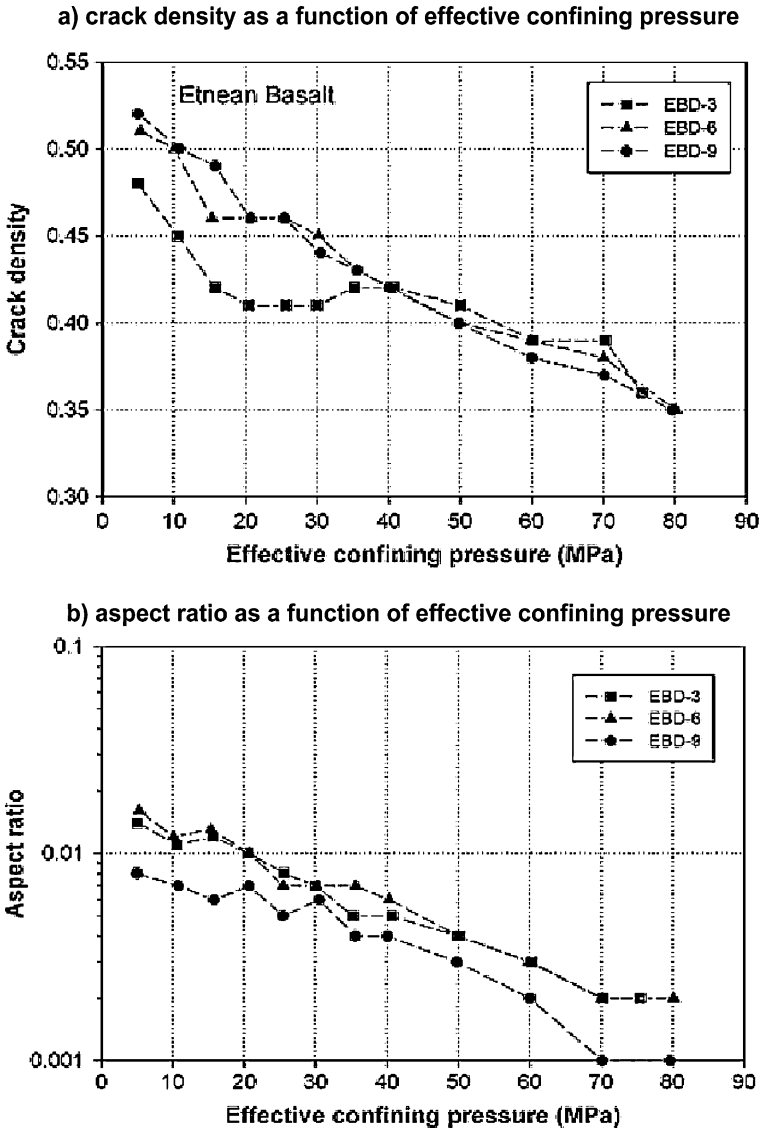

Figure 6

Evolution of crack density (a) and aspect ratio (b) as a function of confining pressure in Etna basalt. Both crack density and aspect ratio were inverted from experimental data presented in Figure 5 and using equations (2) and (3). Matrix elastic parameters were taken as $E = 100$ GPa and $\nu = 0,22$ (i.e., crack-free elastic wave velocities equal to $V_p = 6400$ m/s and $V_s = 3750$ m/s)

data and modelled velocity appears perfect for the same reasons as on Figure 5a. This time, the model crack-free parameters were taken as that of a non-porous calcite aggregate, i.e., $E = 100$ GPa and $\nu = 0.32$. Figure 7b shows the inversion results, i.e., the evolution of crack density (solid diamonds) and aspect ratio (open squares) as a

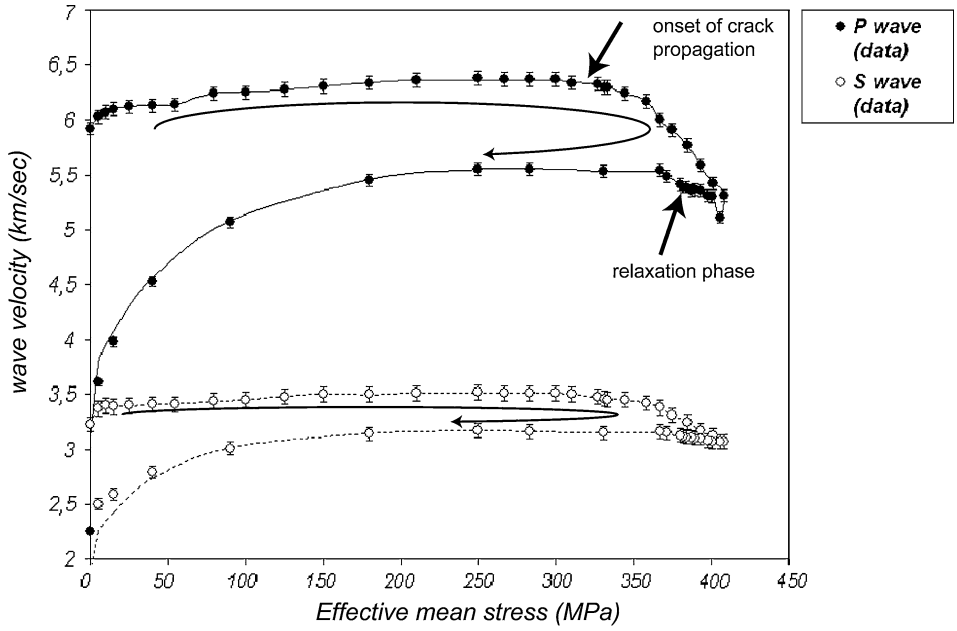
onset of crack propagation
P wave (data)
S wave (data)
relaxation phase
wave velocity (km/sec)
Effective mean stress (MPa)

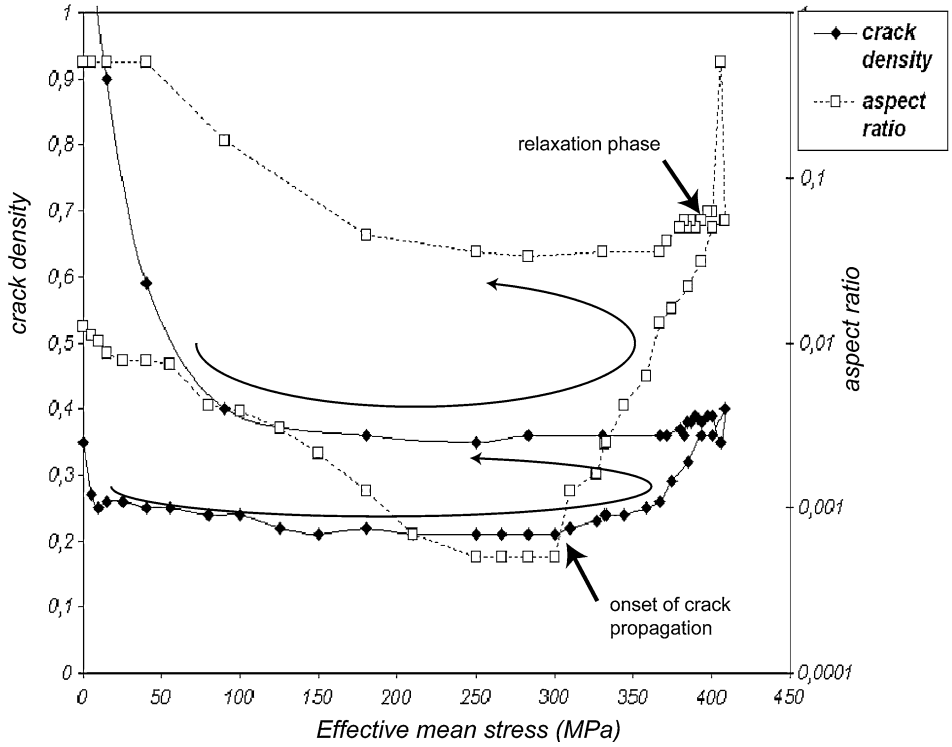
crack density
aspect ratio
relaxation phase
onset of crack propagation
crack density
aspect ratio
Effective mean stress (MPa)

function of effective mean stress. During the first phase, crack density drops from 0.35 to 0.2 while aspect ratio drops again exponentially from 0.01 to lower than 0.001 (more than one order of magnitude) which clearly illustrates crack closure, contact increase in crack surfaces and aperture reduction. During the second phase, crack density increases slightly to 0.5 while aspect ratio increases rapidly to 0.5, revealing that high aspect ratio voids are being opened, which is consistent with microstructural analysis of cataclastic deformation in calcite performed by FREDRICH *et al.* (1989) and SCHUBNEL *et al.* (2005). The aspect ratio last value is probably an artifact of the inversion due to a bad Vp/Vs dataset at the onset of relaxation, because deformation rates were rapid at that point and Vp and Vs measurements were probably distant in time. During the relaxation phase, crack density remains more or less constant while the aspect ratio decreases exponentially again, which is a clear geophysical signature of visco-elastic crack closure and aperture reduction during restrengthening (BEELER and TULLIS, 1997). The fourth phase corresponds to a rapid increase in both crack density and aspect ratio due to stress relief crack propagation and opening. It is interesting to note that the final crack density is larger than 1, although no macroscopic rupture or strain localization band was observed.

3.2 Anisotropic Inversions

Most rocks are characterized by anisotropic crack patterns, often produced by deviatoric stress fields. For example, as a rock body is being deformed during triaxial compression experiments, cracks grow and propagate along preferential orientations, leading to an overall anisotropic elastic pattern (HADLEY, 1975; SCHUBNEL *et al.*, 2003; STANCHITS *et al.*, this issue). However and in the following, because the upper-limit of a non-interactive model is obviously that of instable crack propagation, we do not pretend to deal with coalescence or rupture propagation, but with phenomena prior to these.

3.2.1 Crack density as a function of depth and hydrostatic pressure

Granodiorite samples retrieved from the Nojima fault core were investigated experimentally at room pressure by ZAMORA *et al.* (1999). Elastic wave velocities, measured in the laboratory (500 KHz), are in good agreement with the sonic log

◀

Figure 7

a) Modelled (lines) and data (dots) *P*- and *S*-wave velocities as a function of effective mean stress in Carrara marble. Experiment was performed at $Pc = 260$ MPa confining pressure and $Pp = 10$ MPa. Model crack-free parameters were taken as $E = 100$ GPa and $\nu = 0.32$. b) Evolution of crack density and aspect ratio as a function of effective mean stress. Both crack density and aspect ratio were inverted from experimental data presented on a) and using equations (2) and (3). Arrows indicate the reading and the important phases of the experiment (onset of crack propagation and relaxation phases - cf. SCHUBNEL *et al.*, 2005).

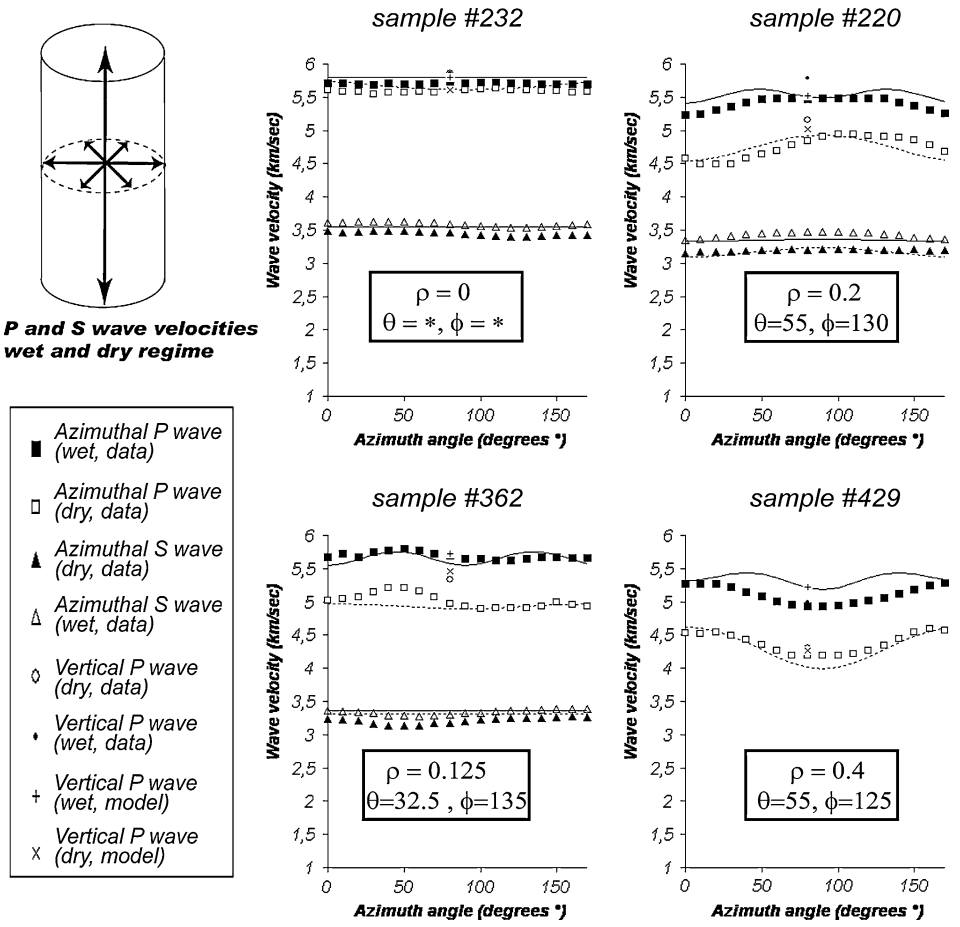

Figure 8

P- and *S*-wave velocity measurements in dry (empty symbols) and wet conditions (plain symbols) of Nojima fault core granodiorite (ZAMORA *et al.,* 1999). Experimental data obtained on four different samples, retrieved at 220, 232, 362 and 429 meters, respectively is presented. *P* waves were measured along the vertical axis and along 18 different directions in the horizontal plane; *S* waves propagating along the vertical axis were measured along 18 different azimuthal polarizations. Modelled velocities for each of these samples are represented by solid and dashed lines. Crack-free elastic parameters were taken as equal to that of sample 232 ($E_o = 85$GPa and $v_o = 0.25$). The inversion outputs both the crack density ρ and the crack fabric orientation (θ, ϕ).

performed during drilling (10 KHz, ZAMORA *et al.*, 1999). In both dry and wet conditions, *P*-wave velocities were measured along the vertical axis and along 18 different azimuthal directions in the horizontal plane; *S*-wave velocities propagating along the vertical axis were measured along 18 different azimuthal polarizations. Figure 8 presents the experimental data (symbols) obtained on four different samples,

retrieved at 220, 232, 362 and 429 meters, respectively. Wet velocities are marked by plain symbols, while dry velocities are marked by empty symbols. For each of these samples, a simultaneous inversion of the dry and wet elastic wave velocity field was performed using equation (9). Crack-free elastic parameters were taken as equal to that of sample 232 ($E_o = 85$ GPa and $v_o = 0.25$), which presented the least amount of damage in the column. The inversion was performed simultaneously in both dry (assuming $\delta/1 + \delta \to 0$) and saturated (assuming $\delta \to 0$) conditions. Modelled azimuthal velocities are represented on Figure 8 as solid and dashed lines. Figure 8 shows that our inversion is reasonable even when the degree of freedom is drastically increased. Indeed, for a given crack density and crack fabric, our modelling effectively mimics both the observed anisotropy pattern and the saturation effect. The retrieved crack density for samples 220, 362 and 429 was 0.2, 0.125 and 0.4, respectively. Fitting of dry data is generally more accurate than fitting of wet data, which might be due to the fact that the incompressible fluid assumption ($\delta \to 0$) is not valid at room pressure. The dip of the distribution is not well constrained due to the paucity of vertical measurements (and the absence of diagonal measurements - see Figures 3 and 4), but is nevertheless in overall agreement with the geological setting (SCHUBNEL, 2002). However, the azimuth of the crack fabric is well constrained and was found to be approximately constant in the column, which is what is intuitively expected in a fault zone, where cracks and damage are aligned parallel to the main fracture plane. This gives us additional confidence in our modelling.

3.2.2 Crack density and aspect ratio evolution as a function of shear stress

Here, we present *P*-wave velocity measurements performed along several directions on a sample of dry Westerly granite during a tri-axial compression (Pc = 50 MPa). The experiment was performed at the USGS at Menlo Park (THOMPSON *et al.*, this issue). The initial *P*-wave velocity field was more or less isotropic and equal to 5.9 km.s^{-1} while final *P*-wave anisotropy exceeded 30%. The non-interactive model can provide a useful tool to study and quantify the first phase of crack propagation, which is stable in triaxial compression experiments. Figure 9a presents a non-exhaustive compilation of the *P*-wave velocity data (symbols, see also THOMPSON *et al.*, this issue) as a function of raypath angle and shear stress steps. The anisotropic pattern is very similar to that of the modelled velocity field for radial cracks presented on Figure 3b, which is as you would expect during the primary phases of a triaxial compression experiment. Modelled velocities are represented by solid and dashed lines. Model crack-free parameters were taken as $E_o = 85$ GPa and $v_o = 0.25$. Data and model velocities fit well. The orientation of the crack fabric is first vertical and then appears to continuously diminish: at 617 MPa, the mean crack fabric dip is only 78° with respect to horizontal, while the crack density increased to 0.44. The inversion, although poorly constrained (only *P*-waves), is stable and coherent. The *P*-wave anisotropy pattern is well reproduced. Figure 9b delineates the evolution

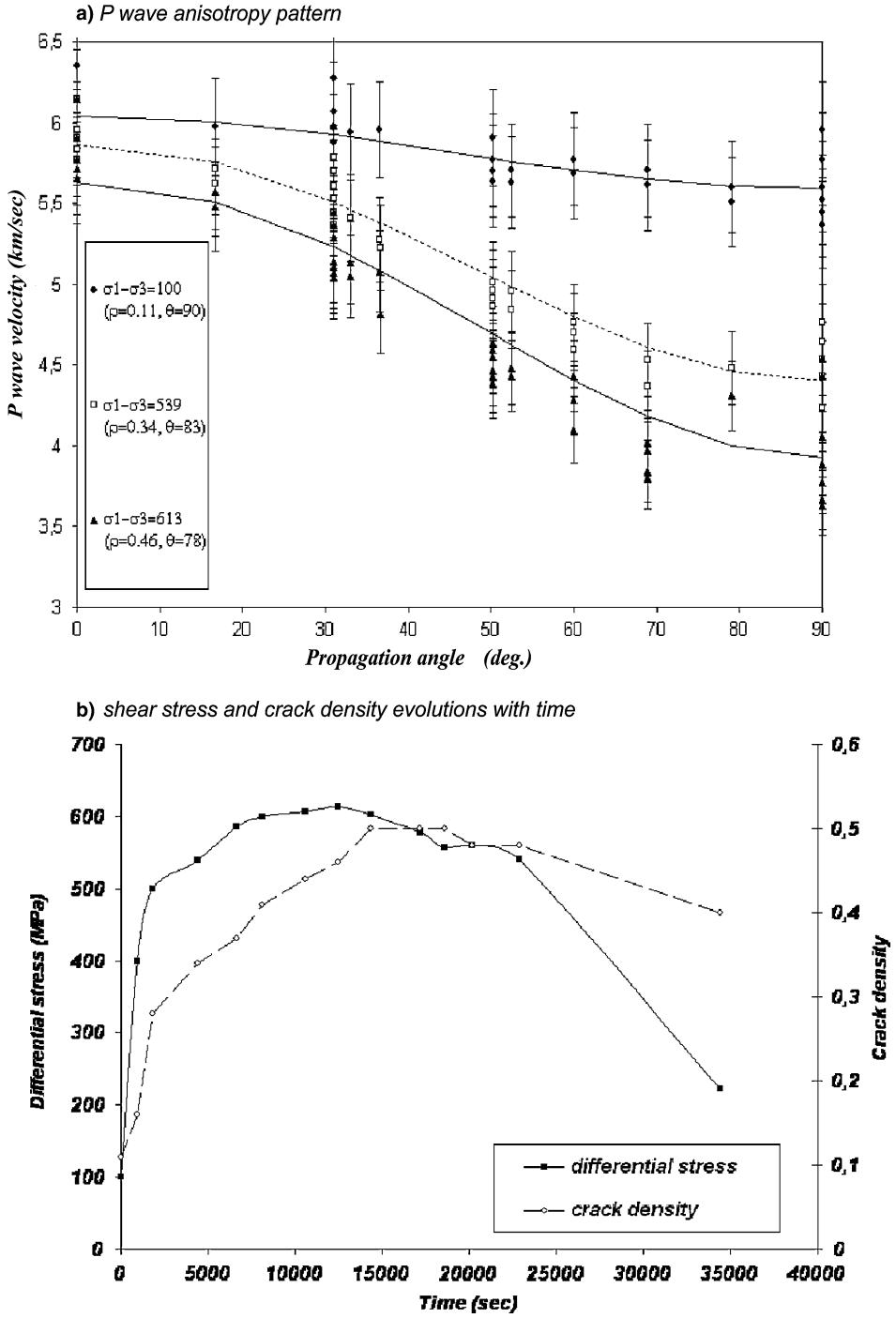
a) P wave anisotropy pattern
P wave velocity (km/sec)
Propagation angle (deg.)
σ1-σ3=100
(p=0.11, θ=90)
σ1-σ3=539
(p=0.34, θ=83)
σ1-σ3=613
(p=0.46, θ=78)
b) shear stress and crack density evolutions with time
Differential stress (MPa)
Crack density
Time (sec)
differential stress
crack density

of shear stress and crack density with time. The system was loaded using Acoustic Emission (AE) feedback (see THOMPSON *et al*., this issue) and one can see that, at first, crack density increased linearly with time. As the system was unloaded, crack density started decreasing, indicating that vertical cracks were closing due to diminishing shear stress. One can see the clear correlation between the two curves. The overall final crack fabric orientation (78°) is in agreement with AE locations, which enabled geophysical imaging of the fracture as it slowly propagated. Although it seems clear that the assumption of homogeneous damage was no longer valid at the end of the test, the inversion continuously output reasonable and physically interpretable results.

4. Discussion and Conclusions

We finally compare our model to that of a numerical simulation of damage evolution using the Particle Flow Code in 3 Dimensions (Itasca Consulting Group). First, a laboratory study was conducted in which a 50 mm cubic sample of Crossland Hill sandstone was subjected to true triaxial loading with velocity measurements taken parallel to each of the principal stress directions. The experiment was performed at Imperial College London (KING, 2002) and then simulated with a distinct element modelling approach using PFC3D. In the numerical experiment, the sample of Crossland Hill sandstone was simulated by an assemblage of 20,000 spherical particles closely packed and bonded together at points of contact. Particle stiffnesses and bond strengths were set such that the macro stiffness and strength of the model matched that of the actual rock. The numerical model and the actual rock sample were both subjected to two episodes of hydrostatic loading up to 100 MPa and then deviatoric loadings. Results of the numerical and laboratory study can be found in HAZZARD and YOUNG (2004). The model was fully dynamic so that changes in wave velocities can be measured with changes in stress. The number of 'cracks' in the model was then directly counted. Figure 10 compares the crack densities calculated from measured velocities and using equations (2)–(3), compared with the crack densities calculated by directly counting the number of cracks (or broken bonds) in the numerical assemblage. To arrive at the curve for 'direct counting', all cracks were assumed to be closed at 100 MPa hydrostatic stress and the number of particle-particle contacts and bonds

◀

Figure 9

a) Modelled (lines) and data (symbols) *P*-wave evolution as a function of shear stress and raypath angle in Westerly granite (THOMPSON *et al.,* 2006). Experiment was performed at $Pc = 50$ MPa confining pressure in dry conditions. Model crack-free parameters were taken as $E = 85$ GPa and $v = 0.25$. Modelled crack density and average crack fabric dip are marked on the legend. b) Shear stress and crack density evolutions as a function of time.

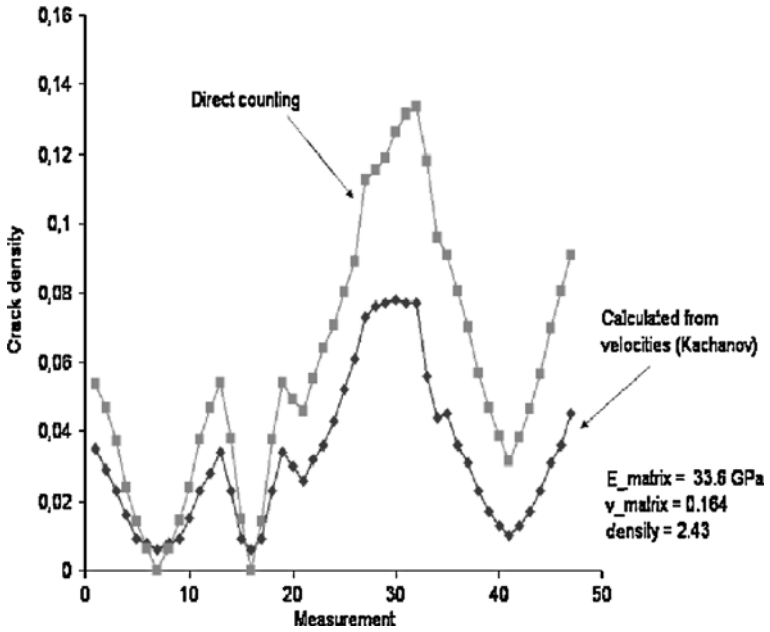

Figure 10
Comparison between PFC model directly observed crack density (crack radii were taken as equal to particles) and Kachanov's model inversion results for Crossland sandstone (KING, 2002; HAZZARD and YOUNG, 2004).

broken relative to this stress state were counted as cracks. Cracks were assumed to have a radius equal to that of the particles. It is clear that there is a fairly good match between the directly counted and calculated crack densities, which validates the modelling. However, the direct counting seems to systematically overestimate the crack density and the deviation between theoretical and numerical modelling increases with increasing crack density. This is probably due to the fact the crack radii are overestimated when taken as equal to the particle's radius. Real fractures also have shapes which are complex in detail, and this may be an additional reason for the differences shown in Figure 10. This may also reflect the fact that the material is no longer isotropic and that a Transversely Isotropic formulation might have produced better results.

The main question that remains is that of the significance of the fit between the laboratory or numerical and theoretical data. In general, this fit (e.g., in Fig. 5) is excellent and clearly, *P*- and *S*-wave velocities will in general be smoothly varying functions of the various parameters involved, in Figure 5a the effective confining pressure for example. If this is the case, then we can expect to describe any such curve with few parameters (i.e., the true empirical curve contains relatively few degrees of freedom). If the true number of degrees of freedom in the model is comparable to the true number of degrees of freedom in the data, then an excellent

fit will always be found - but this is not necessarily significant. However, only a relatively good model which relies on good parameters will systematically output, using an inverse method, a physically understandable and expected evolution of the fitting parameters. In our case, the systematic decrease in crack density with confining pressure illustrates a decrease in the crack's apparent radii c as crack density evolves with $\sim c^3$. An increase in crack density also helps in quantifying crack growth. This can also be interpreted as a variation of the crack surfaces contact areas as cracks are being closed or opened, respectively. Even more so, the recovered evolution of aspect ratio shows an exponentially decreasing aspect ratio (and therefore aperture) with confining pressure which is also consistent with current mechanical theories of crack closure (KASELOW and SHAPIRO, 2004). The crack fabric orientations we recovered, when the rock was anisotropic, are also consistent with *in situ* geophysical imaging.

In conclusion, by using a non-interactive crack effective medium theory as a fundamental tool, it is possible to calculate the cracked rock dry and wet elastic properties in terms of a crack density tensor, average crack aspect ratio and mean crack fabric orientation using the solid grains and fluid elastic properties solely. Using the same method, both the anisotropy and shear-wave splitting of elastic waves can be derived. Two simple crack distributions have been considered for which the predicted anisotropy depends strongly on the saturation, reaching 60% in the dry case.

In the isotropic case, KACHANOV's (1994) model was used to invert elastic wave velocities and infer both crack density and aspect ratio evolutions. Inversion results were coherent in terms of crack density and aperture evolutions. A systematic decrease in crack density with confining pressure illustrated a decrease in the crack's apparent radii c. An increase in crack density can facilitate the precise quantification of crack growth (FORTIN *et al.*, 2006). Using such an inversion tool opens the door in linking elastic propertie's variations to permeability, as pointed out GUÉGUEN and SCHUBNEL (2003) or BENSON *et al.* 2006.

Inversion results agreed very well with the data and were consistent with the microstructure of the different rocks investigated here. That the theoretical curves in Figures 5a and 7a so closely follow the minor fluctuations in the empirical data curves might also suggest that the data are being overfitted. Obviously, if the first step in verifying a theoretical model is to compare it directly to data, a logical next step would be to perform a variance, covariance analysis in order to more reliably assess what the fit between data and model really means. It needs to be pointed out that for crack densities larger than 0.5, the predictions of the model are less accurate but would nevertheless remain within the same physical trend, which is a major difference with the Self-Consistent method (O'CONNELL and BUDIANSKY, 1975). A natural extension of this work would be to incorporate inversion of

porosity into the model. Unfortunately, such extensive laboratory data is very rare in the literature.

Acknowledgements

The authors would like to acknowledge MARIA ZAMORA, ANNE-MARIE BOULIER and PHILIPPE PEZARD for providing the data on the Nojima fault core. SERGIO VINCIGUERRA, CONCETTA TROVATO and PHILIP MEREDITH provided the UCL data and are duly thanked. DAVID LOCKNER, LUIGI BURLINI and JÉRÔME FORTIN assisted in acquiring the data on Westerly granite and Carrara marble, respectively. This work was developed thanks to many useful discussions with MARK KACHANOV, IAN JACKSON and YVES GUÉGUEN. Additional and useful comments were provided by DAVID COLLINS and FARZINE NASSERI. We would also like to thank our two reviewers, ERIK SAENGER and ROLAND ROBERTS, for their very constructive comments which helped to greatly improve the quality of this manuscript. This study was partially supported by an NSERC discovery grant obtained by Prof. R. PAUL YOUNG.

Appendix I

Elastic Deformation of a Single Penny-shaped Crack

For a single penny-shaped crack under a uniform normal load p or shear stress τ, the elastic normal and shear displacements of the crack surfaces are not equal (and thus there can be a non-collinearity between the stress and displacement vectors). Such elastic displacements $\langle \mathbf{b} \rangle$ can be written respectively as (KACHANOV, 1994):

$$\langle \mathbf{b} \rangle = \begin{cases} \langle b_n \rangle &= \frac{16(1-\nu^2)c}{3\pi E} p \\ \langle b_\tau \rangle &= \frac{16(1-\nu^2)c}{3\pi(1-\nu/2)E} \tau \end{cases} \tag{12}$$

where c is the crack radius, E and ν the matrix YOUNG's modulus and Poisson ratio respectively. In the case of a crack filled up with fluid, an applied stress on the crack surface will generate a pore pressure variation Δp_f. Considering the crack aspect ratio $\zeta = w/c$, and assuming that $w \ll c$, the volume variation of the crack is mainly related to a change in its aperture. Thus the total traction applied on the crack surface is $\mathbf{n}.\sigma.\mathbf{n} + \Delta p_f$. From equation (12), one obtains:

$$\langle \Delta b_n \rangle = \frac{16(1-\nu^2)c}{3\pi E} (\mathbf{n} \cdot \sigma \cdot \mathbf{n} + \Delta p_f). \tag{13}$$

Considering that the fluid mass is constant, the variation in fluid density, volume and aperture are linked:

$$\frac{\Delta\varrho}{\varrho_o} = -\frac{\Delta V}{V_o} = \frac{-\langle \Delta w \rangle}{\langle w \rangle} = -\frac{\langle \Delta b_n \rangle}{\langle w \rangle}. \tag{14}$$

Remembering that $\Delta p_f = -K_f \frac{\Delta\varrho}{\varrho_o}$, the crack normal compliance B_N is such that (KACHANOV, 1994):

$$\frac{B_N}{B_T} = \left(1 - \frac{\nu_0}{2}\right) \frac{\delta}{1+\delta}, \tag{15}$$

where δ is given by equation (5) of the main text.

REFERENCES

ANDERSON, D.L., MINSTER, B., and COLE, D. (1974), *The effect of oriented cracks on seismic velocities*, JGR *79*, 4011–4015.

BEELER, N.M. and TULLIS, T.E. (1997), *The roles of time and displacement in velocity dependent volumetric strain of fault zones*, JGR *102*, 22595–22609.

BENSON, P. M. (2004), *Experimental study of void space, permeability and elastic anisotropy in crustal rock under ambient and hydrostatic pressure*, Ph.D. Thesis, 272 pp., University of London, London.

BENSON, P., SCHUBNEL, A., VINCIGUERRA, S., TROVATO, C., MEREDITH, P., and YOUNG, R.P. (2006), *Modelling the permeability evolution of micro-cracked rocks from elastic wave velocity inversion at elevated hydrostatic pressure*, JGR *111*, in press.

BRACE, W.F., WALSH, J.B., and FRANGOS, W.T. (1968), *Permeability of granite under high pressure*, JGR *73*, 2225–2236.

BERRYMAN, J.G. (1992), *Single-scattering approxmations for coefficient in Biot equations of poroelasticity*, J. acoustical Soc. Am. *92*, 551–571.

BROWN, R. and KORRINGA, J. (1975), *On the dependence of the elastic properties of a porous rock on the compressibility of the pore fluid*, Geophysics *40*, 608–616.

CHENG, C.H. and TOKSÖZ, M.N. (1979), *Inversion of seismic velocities for the pore aspect ratio spectrum of a rock*, JGR *84*, 7533–7543.

CHUN, K.-Y., HENDERSON, G. A., and LIU, J. (2004), *Temporal changes in P-wave attenuation in the Loma Prieta rupture zone*, JGR *109*, B02317, doi:10.1029/2003JB002498.

CLEARY, M.P., CHEN, I.W. and LEE S.M. (1980), *Self-consistent techniques for heterogeneous media*, J. Engin. Div. *106*, 861–887.

ESHELBY, J.D. (1957), *The determination of the elastic field for an elliptical inclusion and related problems*, Proc. R. Soc. London *241,* 376–396.

FORTIN, J. (2005), Compaction homogène et compaction localisée des roches poreuses, PhD. thesis, Université Pierre et Marie Curie, Paris, France.

FORTIN J., GUÉGUEN, Y., and SCHUBNEL, A. (2006), *Consequences of pore collapse and grain crushing on ultrasonic velocities and Vp/Vs*, JGR, in press.

FREDRICH, J.T., EVANS, B., and WONG, T.-F. (1989), *Micromechanics of the brittle to plastic transition in Carrara marble*, JGR *94*, 4129–4145.

GAO, Y. and CRAMPIN, S. (2004), *Observations of stress relaxation before earthquakes*, Geophys. J. Int. *157*, 578–582.

GUÉGUEN, Y. and SCHUBNEL, A. (2003), *Elastic wave velocities and permeability of cracked rocks*, Tectonophysics *370*, 163–176.

HADLEY, K. (1975), *Azimuthal variation of dilatancy*, JGR *80*, 4845–4850.

HAZZARD, J.F. and YOUNG, R.P. (2004), *Numerical investigation of induced cracking and seismic velocity changes in brittle rock*, GRL *31*, Art. No. L01604.

HUDSON, J.A. (1981), *Wave speeds and attenuation of elastic waves in material containing cracks*, Geophys. J. R. Astr. Soc. *64*, 133–150.

HUDSON, J.A. (1982), *Overall properties of a cracked solid*, Math. Proc. Cambridge Phil. Soc. *88*, 371–384.

HUDSON, J.A. (1986), A higher order approximation to the wave propagation constants for a cracked solids, Geophys. J. R. Astr. Soc. *87*, 265–274.

KACHANOV, M. (1994), *Elastic solids with many cracks and related problems*, Adv. Appl.Mech. *30* 259–445.

KASELOW, A. and SHAPIRO, S.A. (2004), *Stress sensitivity of elastic moduli and electrical resistivity in porous rocks*, J. of Geophy. Engin *1*, 1–11.

KERN, H. (1978), *The effect of high temperature and high confining pressure on compressional wave velocities in quartz bearing and quartz free igneous and metamorphic rocks*, Tectonophysics *44*, 185–203.

KERN, H., LIU, B., and POPP, T. (1997), *Relationship between anisotropy of P- and S-wave velocities and anisotropy of attenuation in serpentinite and amphibolite*, JGR *102*, 3051–3065.

KING, M.S. (2002), *Elastic wave propagation in and permeability for rocks with multiple parallel fractures*, Int. J. Rock Mech. Min. Sci. *39*, 1033–1043.

LE RAVALEC, M. and GUÉGUEN, Y. (1996), *High and low frequency elastic moduli for a saturated porous/cracked rock - Differential self-consistent and poroelastic theories*, Geophys. *61*, 1080–1094.

MAVKO, G. and NUR, A. (1975), *Melt squirt in the asthenosphere*, JGR *80*, 1444–1448.

MAVKO, G. and JIZBA, D. (1991), *Estimating grain-scale fluid effects on velocity dispersion in rocks*, Geophysics *56,* 1940–1949.

MAVKO, G., MUKERJI, T., and DVORKIN, J. In *The Rock Physics Handbook* (Cambridge University Press 1998), 329 pp.

MILLER, S. A. (2002), *Properties of large ruptures and the dynamical influence of fluids on earthquakes and faulting*, JGR *107(B9)*, 2182, doi:10.1029/2000JB000032.

NASSERI, M.H.B., MOHANTY, B., and YOUNG, R.P. (2006), *Fracture toughness measurements and acoustic emission activity in brittle rocks*, Pure Appl. Geophys. this issue.

NISHIZAWA, O. (1982), *Seismic velocity anisotropy in a medium containing oriented cracks: Transverse isotropy case*, J. Phys. Earth *30,* 331–347.

O'CONNELL, R. and BUDIANSKY, B. (1974), *Seismic velocities in dry and saturated rocks*, JGR *79,* 5412–5426.

O'CONNELL, R. and BUDIANSKY, B. (1977), *Viscoelastic properties of fluid saturated cracked solids*, JGR *82,* 5719–5736.

ORLOWSKY, B., SAEGER, E.H., GUÉGUEN, Y., and SHAPIRO, S.A. (2003), *Effects of parallel crack distributions on effective elastic properties — a numerical study*, Internat. J. Fract. *124*, 171–178.

SAENGER, E.H., KRUGER, O.S., and SHAPIRO, S.A. (2004), *Effective elastic properties of randomly fractured soils: 3-D numerical experiments*, Geophys. Prosp. *52*, 183–195.

SAYERS, C.M. and KACHANOV, M. (1991), *A simple technique for finding effective elastic constants of cracked solids for arbitrary crack orientation statistics*, Int.J Sol. Struct. *12*, 81–97.

SAYERS, C.M. and KACHANOV, M. (1995), *Microcrack induced elastic wave anisotropy of brittle rocks*, JGR *100*, 4149–4156.

SCHOENBERG, M. and SAYERS, C.M. (1995), *Seismic anisotropy of fractured rock*, Geophysics *60*, 204–211.

SCHUBNEL, A. (2002), *Mécanique de la dilatance et de la compaction des roches de la croûte*, Ph.D. Thesis of *Institut de Physique du Globe de Paris*, 229pp.

SCHUBNEL, A., NISHIZAWA, O., MASUDA, K., LEI, X.J., XUE, Z. and GUÉGUEN, Y. (2003), *Velocity measurements and crack density determination during Wet Triaxial Experiments on Oshima and Toki Granites*, Pure Appl. Geophy. *160*, 869–887.

SCHUBNEL, A. and GUÉGUEN, Y. (2003), *Dispersion and anisotropy in cracked rocks*, JGR *108*, 2101, doi:10.1029/2002JB001824.

SCHUBNEL A., FORTIN, J., BURLINI L., and GUÉGUEN, Y. (2005), *Damage and recovery of calcite rocks deformed in the cataclastic regime*. In Geological Society of London special publications on *High Strain Zones* (eds. by Bruhn, D. and Burlini, L.) *245*, 203–221.

SIMMONS, G. and BRACE, W.F. (1965), *Comparison of static and dynamic measurements of compressibility of rocks*, JGR *70*, 5649–5656.

SIMMONS, G., TODD, T., and BALRIDGE, W.S. (1975), *Toward a quantitative relationship between elastic properties and cracks in low porosity rocks*, AM. J. Sci. *275*, 318–345.

SOGA, N., MIZUTANI, H., SPETZLER, H. and MARTIN, R. J. III. (1978),*The effect of dilatancy on velocity anisotropy in Westerly Granite*, JGR *83*, 4451–4458.

STANCHITS, S., VINCIGUERRA, S., and DRESEN, G. (2006), *Ultrasonic velocities, acoustic emission characteristics and crack damage of basalt and granite*, Pure Appl. Geophys. this issue.

THOMPSON, B.D., YOUNG, R.P., and LOCKNER D.A. (2006), *Observations of fracture in Westerly granite under AE feedback and constant strain rate loading: Nucleation, quasi-static propagation, and the transition to unstable fracture propagation*, Pure Appl. Geophys. this issue.

VOLTI, T. and CRAMPIN, S. (2003), *A four-year study of shear-wave splitting in Iceland: 2. Temporal changes before earthquakes and volcanic eruptions*. In Geological Society of London special publications on *New Insights into Structural Interpretation and Modelling* (ed. Nieuwland, D.A.) *212*, 135–149.

WALSH, J.B. (1965), *The effect of cracks on the compressibility of rock*, JGR *70*, 381–389.

ZAMORA, M., PEZZARD, P.A., and ITO, H. (1999), *Anisotropy of elastic properties of granites from the Hirabayashi borehole, Japan*, internal note, GSJ/USGS.

(Received May 4, 2005, revised October 28, 2005, accepted October 29, 2005)